Supporting Information

Isomeric Co(II) paraCEST agents as pH responsive MRI probes

Christopher J. Bond, Roy Cineus, Joseph Spernyak, Alexander Y. Nazarenko, Janet R. Morrow*

Table of Contents

Materials and Methods.

Materials. 1,4,8,11-tetraazacyclotetradecane (CYCLAM,98%) was purchased from Strem Chemicals. 2-Bromoacetamide (98%) was purchased from Acros organics. $CoCl_2 \bullet 6H_20$ was purchased from Alfa Aesar. The ligand, 1,4,8,11-tetrakis(carbamoylmethyl)-1,4,8,11-tetraazacyclotetradecane (CCRM), and $[Co(1,4\text{-}CCRM)]Cl_2$ were synthesized as reported.[1] $[Co(1,8\text{-}CCRM)]Cl_2$ was synthesized from $[Co(1,4\text{-}CCRM)]Cl_2$ by heating in aqueous solution for two hours at 100 ^oC.

Crystal Information. Single-crystal X-ray data of the complexes were collected on a Bruker VENTURE Photon-100 CMOS diffractometer at 173 K with APEX 2 software suite. The absorption correction was applied using multiscan *SADABS2014*/5 (Bruker,2014/5) and the structures were solved by the direct methods using SHELXT,85 and were refined using the SHELXL-2014 program package. Computer programs: *SAINT* v8.34A (Bruker, 2013), XT (Sheldrick, 2015), XL (Sheldrick, 2008), Olex2 (Dolomanov *et al.*, 2009).

NMR spectroscopy. ^{1}H NMR was acquired on a Varian 500 MHz NMR at 25^oC unless otherwise stated. Spectra were processed on ACD lab software.

CEST Experiments. CEST data were acquired on a Varian 500 MHz NMR spectrometer with a presaturation pulse power (B_1) of (29 μT) applied for 2 s at 37 °C unless otherwise stated. Solutions contained 10 mM complex, 20 mM HEPES buffer, and 100 mM NaCl, and at pH values between 6.8 and 7.9. Data were acquired in 1 ppm increments and plotted as normalized water signal intensity (M_Z/M_0 %) against frequency offset (ppm) to generate CEST spectra. Data was processed and plotted by using Microsoft excel.

Determination of Exchange Rate Constants by Omega Plots and HW-QUESP method.

The omega plot method[2] was used for determination of exchange rate constants. Magnetization of the on (M_Z) and off-resonance (M_0) frequencies were acquired and compared over saturation powers 19-29 μT. The values of the "on" and "off" frequencies were collected with a presaturation pulse applied for 2 seconds at 37°C. The rate constant, k_b, is determined by taking the x-intercept ($-1 / k_b^2$) of the regression line generated from the plot of $M_Z /(M_0 - M_Z)$ against $1/\omega^2$ (in rad/s) and converted to get a value in Hz. Samples used contained 10mM complex, 20mM HEPES buffer, and 100mM NaCl.

The HW-QUESP method[3] was performed for comparison to the omega plot method. Both methods produced very similar exchange rate constant values.

Evans method for determination of magnetic moments.

Evans method was used for measurement of magnetic susceptibility as described in literature.[4-5] Three independently measured values were averaged. In a typical experiment, a solution of 10 mM Co(II) complex in water, neutral pH (6-8), containing 5% tert-butanol (v/v) was placed in an NMR tube insert, while a reference solution of 5% tert-butanol (v/v) in deuterium oxide was contained in the NMR tube. The mass susceptibility χ_g was calculated using Eq. 1, where Δf is the shift in frequency (Hz); ν_0 is the operating frequency of NMR spectrometer (Hz); m is the concentration of the substance (g/mL). The solvent correction was taken into account (Eq. 1). The molar susceptibility was calculated by multiplying by the molar mass. Then the paramagnetic molar susceptibility χ_M^p was calculated from subtracting the

diamagnetic susceptibility contribution (χ_M^{dia}) in eq. 2. This was used to calculate the effective magnetic moment μ_{eff} (Eq. 3).

$$\chi_g = \frac{3\Delta f}{4\pi \nu_0 m} + \chi_o \qquad \text{Eq. 1}$$

Example calculation for Co(II) complex where: $\Delta f =$ X Hz, T=298, [complex]=0.0100 mol/L, spectrometer frequency (ν_o) = 500 MHz, M.W. = 558.4 g/mol

Mass susceptibility = [(3 x 197.5 Hz]/[(4π x 500,000,000 Hz x 0.005584 g/mL)] +(-6.5 x 10^{-7}) = 1.69*10^{-5}

1. (Measured) molar susceptibility (multiply by molar mass of 558.4 g/mol)

χ_M = 0.00943 emu mol^{-1}

$$\chi_M^p = \chi_M - \chi_M^{dia} \qquad \text{Eq. 2}$$

$$\mu_{eff} = 2.83(\chi_M^p T)^{1/2} \qquad \text{Eq. 3}$$

where χ_M^{dia}= -(M.W/2) x 10^{-6}=-0.00024319 emu mol^{-1}

2. (χ_M^p) = (0.00943) - (-0.00024319) = 0.00968emu mol^{-1}
3. $\mu_{eff} = 2.83(\chi_M^p T)^{1/2}$ = 2.83 [0.00941831x298]$^{1/2}$

= 4.77 Bohr magneton

Dissociation studies in the presence of H^+, anions, Zn^{2+}, and Cu^{2+}.

^{1}H NMR samples of 20 mM complex were incubated with 100 mM NaCl and 3 mM 3-(trimethylsilyl)-1-propanesulfonic acid sodium salt as a standard. For experiments done under acidic conditions, the pD was adjusted to between 3.5 and 4.0. For studies with competing anions, 25 mM K_2CO_3 and 0.40 mM K_2HPO_4 were studied at pH values between pD 7.0 and 7.5. To study inertness to transmetalation, solutions were tested with 20 mM $ZnCl_2$ at pD 6.5−7.0. All samples were incubated at 37 °C for a twelve-hour period, and determination of dissociation was done by measuring the relative intensities of diamagnetic peaks to the internal diamagnetic standard, to calculate how much ligand had dissociated.

For dissociation resulting from Cu^{2+} trans-metalation, solutions of 100 µM Co(II) complex and 20 mM pH 6 MES buffer, were combined with 1, 2, or 4 equivalents of $Cu(NO_3)_2$ (aq), and the formation of $[Cu(CCRM)]^{2+}$ was observed over time at one minute intervals by UV-vis spectrometry at 304 nm. Percent dissociation was calculated using the following: absorbance of $[Co(CCRM)]^{2+}$ and $Cu(NO_3)_2$ solution/absorbance $[Cu(CCRM)]^{2+}$ after 6 hours, multiplied by 100%.

CEST Studies in chicken homogenate

Samples of 0.25-0.3g of homogenized chicken thigh were soaked in 300 uL solutions with approximately 50 mM $Co(CCRM)Cl_2$ complex, 20 mM pH 7.4 HEPES buffer, for 48 h under refrigeration. During the first 24 h, the pH of the samples was checked and adjusted with a 1M NaOH solution until the pH of the

sample was approximately 7.4. Z-spectra were acquired on a Varian 400 and 500 MHz NMR spectrometer with a presaturation pulse power (B_1) of (29 μT, 19 μT, or 12 μT) applied for 2 s at 37 °C unless otherwise stated. Data were acquired in 1 ppm increments and plotted as normalized water signal intensity (M_Z/M_0 %) against frequency offset (ppm) to generate Z-spectra. $CEST_{asymmetry}$ was calculated by plotting $(Mz/M_0)_{\text{negative frequency}} - (Mz/M_0)_{\text{positive frequency}}$ against offset from bulk water which was set at 0 ppm. Data was processed and plotted on Microsoft excel.

Phantom imaging at 4.7 T. CEST imaging was performed on a 4.7 Tesla MRI scanner (ParaVision 3.0.2, Bruker Biospin, Billerica MA) using a 60 cm (I.D.) gradient insert and a 35 mm (I.D.) quadrature radiofrequency coil (m2m imaging, Cleveland, OH). Temperature was maintained at 37 ^{o}C during imaging using an MR-compatible heating system (SA Instruments, Stony Brook, NY). Samples were imaged using a pair of spoiled gradient echo scans with the following acquisition parameters: TE/TR = 2.1/5010 ms, flip angle = 90 deg, matrix = 128 x 128, FOV = 32 x 32cm, 2 mm slice thickness. Buffer alone and deionized water samples were included as negative controls. CEST saturation images (M_S) were acquired with five pre-saturation pulses (12μT, 1 s duration, 200 μs interpulse delay). Three sets of 124 ppm offsets were acquired, and two sets of 44 ppm offsets were acquired. Control (M_0) images were acquired under identical conditions except the power of presaturation pulses were reduced to 0 μT. Signal intensities were sampled by region of interest analysis and normalized to the buffer-alone signal intensity. CEST reduction values were calculated as: percent reduction = $1 - M_S/M_0$.

Crystal Structure Information.

Table S1: Structure (1) Corresponds to [Co(1,8-CCRM)], while (2) and (3) correspond to [Co(1,4-CCRM)], Crystal data, data collection and structure refinement details are summarized below.

	(1)	(2)	(3)
Crystal data			
Chemical formula	$C_{18}H_{36}CoN_8O_4 \cdot 2(CNS)$	$C_{18}H_{36}CoN_8O_4 \cdot 3(H_2O) \cdot C_4CoN_4S_4$	$C_{18}H_{36}CoN_8O_4 \cdot 2(ClO_4) \cdot H_2O$
M_r	603.64	832.77	704.39
Crystal system, space group	Monoclinic, $P2_1/n$	Triclinic, $P\bar{1}$	Triclinic, $P\bar{1}$
Temperature (K)	173	173	173
a, b, c (Å)	8.7005 (6), 12.9672 (11), 11.9397 (11)	10.0766 (5), 10.7225 (6), 17.5231 (9)	8.8541 (6), 9.9859 (8), 17.8607 (14)
α, β, γ (°)	90, 104.610 (3), 90	75.030 (2), 74.215 (2), 82.412 (2)	92.863 (2), 103.261 (2), 111.451 (2)
V (Å^3)	1303.49 (19)	1756.18 (16)	1414.90 (19)
Z	2	2	2
Radiation type	Mo $K\alpha$	Mo $K\alpha$	Mo $K\alpha$
μ (mm^{-1})	0.87	1.24	0.87
Crystal size (mm)	0.32 × 0.18 × 0.16	0.2 × 0.2 × 0.1	0.6 × 0.53 × 0.34
Data collection			
Diffractometer	Bruker *Photon-100 CMOS*	Bruker *Photon-100 CMOS*	Bruker *Photon-100 CMOS*
Absorption correction	Multi-scan *SADABS2014*/5 (Bruker,2014/5) was used for absorption correction. wR2(int) was 0.0527 before and 0.0486 after correction. The Ratio of minimum to maximum transmission is 0.8908. The λ/2 correction factor is 0.00150.	Multi-scan *SADABS2014*/5 (Bruker,2014/5) was used for absorption correction. wR2(int) was 0.0609 before and 0.0537 after correction. The Ratio of minimum to maximum transmission is 0.9064. The λ/2 correction factor is 0.00150.	Multi-scan *SADABS2014*/5 (Bruker,2014/5) was used for absorption correction. wR2(int) was 0.0614 before and 0.0532 after correction. The Ratio of minimum to maximum transmission is 0.7580. The λ/2 correction factor is 0.00150.
T_{min}, T_{max}	0.816, 0.916	0.826, 0.911	0.632, 0.834
No. of measured, independent and observed [$I > 2\sigma(I)$] reflections	56822, 4540, 3978	76295, 7331, 5582	94139, 9344, 8231
R_{int}	0.032	0.057	0.040

$(\sin\theta/\lambda)_{max}$ (Å^{-1})	0.747	0.631	0.735
Refinement (table X continued)			
$R[F^2 > 2\sigma(F^2)]$, $wR(F^2)$, S	0.029, 0.077, 1.04	0.033, 0.078, 1.02	0.031, 0.082, 1.05
No. of reflections	4540	7331	9344
No. of parameters	185	457	426
No. of restraints	0	36	52
H-atom treatment	H atoms treated by a mixture of independent and constrained refinement	H atoms treated by a mixture of independent and constrained refinement	H atoms treated by a mixture of independent and constrained refinement
$\Delta\rangle_{max}$, $\Delta\rangle_{min}$ (e Å^{-3})	0.54, -0.39	0.41, -0.49	0.53, -0.42

Crystal data for 1 (CCDC No. 1949780). $C_{18}H_{36}CoN_8O_4{\cdot}2(CNS)$, M = 603.64, monoclinic, a = 8.7005 (6), b= 12.9672(11), c = 11.9397(11) Å, β (°) = 104.610(3), V = 3741.0(9) Å^3, T = 173 K, space group = $P2_1/n$ (no.14), Z = 2, 56822 reflections measured, 4540 unique (R^{int} = 0.032), which were used in all calculations. $R[F^2 > 2\sigma(F^2)]$, $wR(F^2)$, = 0.029, 0.077.[6-9]

Crystal data for 2 (CCDC No. 1949781). $C_{18}H_{36}CoN_8O_4{\cdot}3(H_2O){\cdot}$ $Co(CNS)_4$, M = 832.77, triclinic, a = 10.0766(5), b= 10.7225(6), c = 17.5231(9) Å, α, β, γ (°) = 75.030 (2), 74.215 (2), 82.412 (2), V = 1756.18 (16) Å^3, T = 173 K, space group = $P\bar{1}$ (no.2), Z = 2, 76295 reflections measured, 7331 unique (R^{int} = 0.057), which were used in all calculations. $R[F^2 > 2\sigma(F^2)]$, $wR(F^2)$, = 0.033, 0.078.[6-9]

Crystal data for 3 (CCDC No. 1949782). $C_{18}H_{36}CoN_8O_4{\cdot}2(ClO_4){\cdot}H_2O$, M = 704.39, triclinic, a = 8.8541(6), b= 9.9859(8), c = 17.8607 (14)Å, α, β, γ (°) = 92.863(2), 103.261(2), 111.451(2), V = 1414.90(19)Å^3, T = 173 K, space group = $P\bar{1}$ (no.2), Z = 2, 94139 reflections measured, 9344 unique (R^{int} = 0.04), which were used in all calculations. $R[F^2 > 2\sigma(F^2)]$, $wR(F^2)$, = 0.031, 0.082.[6-9]

Geometry. All esds (except the esd in the dihedral angle between two l.s. planes) are estimated using the full covariance matrix. The cell esds are taken into account individually in the estimation of esds in distances, angles and torsion angles; correlations between esds in cell parameters are only used when they are defined by crystal symmetry. An approximate (isotropic) treatment of cell esds is used for estimating esds involving l.s. planes.

Paramagnetic complexes and ^{1}H NMR spectroscopy

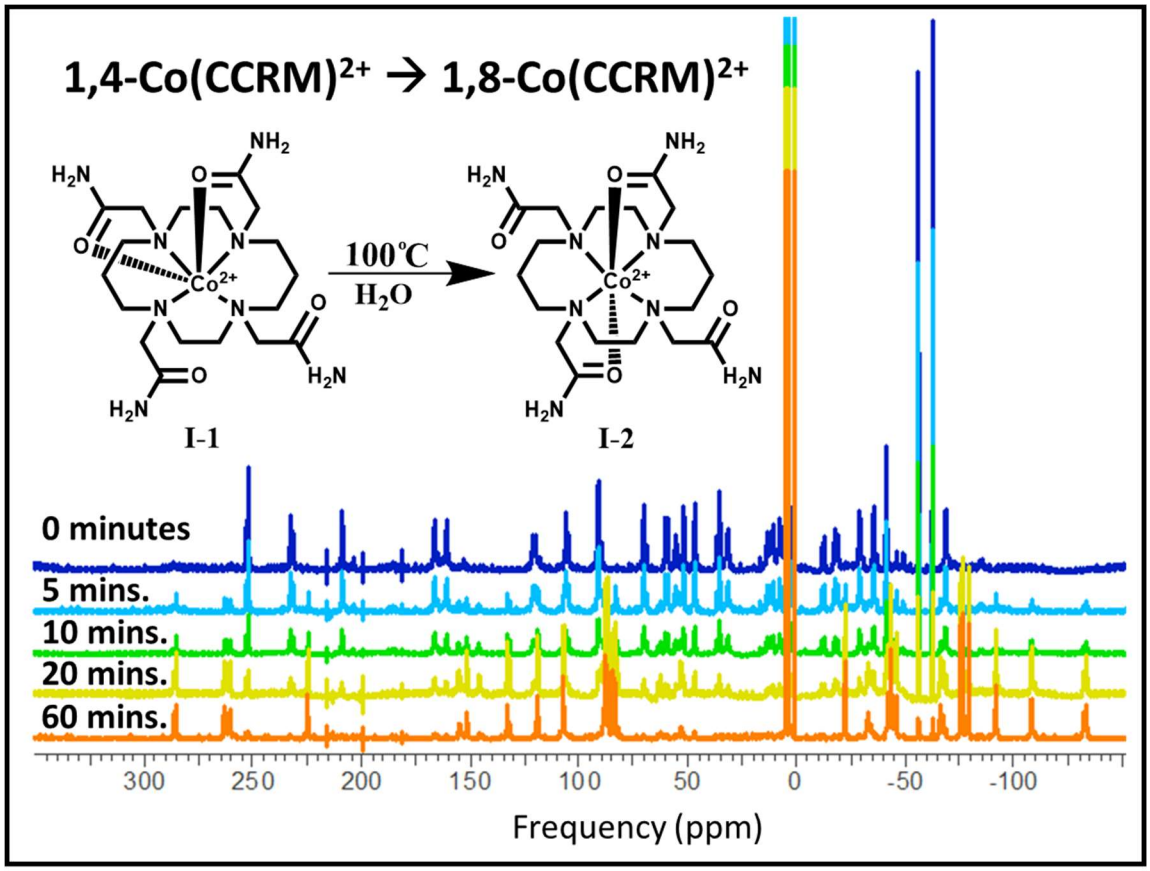

Figure S1: Overlaid ^{1}H NMR spectra of $[Co(CCRM)]^{2+}$ after 0, 5, 10, 20 and 60 minutes of heating, to observe the conversion of the two isomers by monitoring the appearance and disappearance of peaks associated with each isomer. ^{1}H NMR spectra were taken at room temperature, 500 MHz NMR, in D_2O.

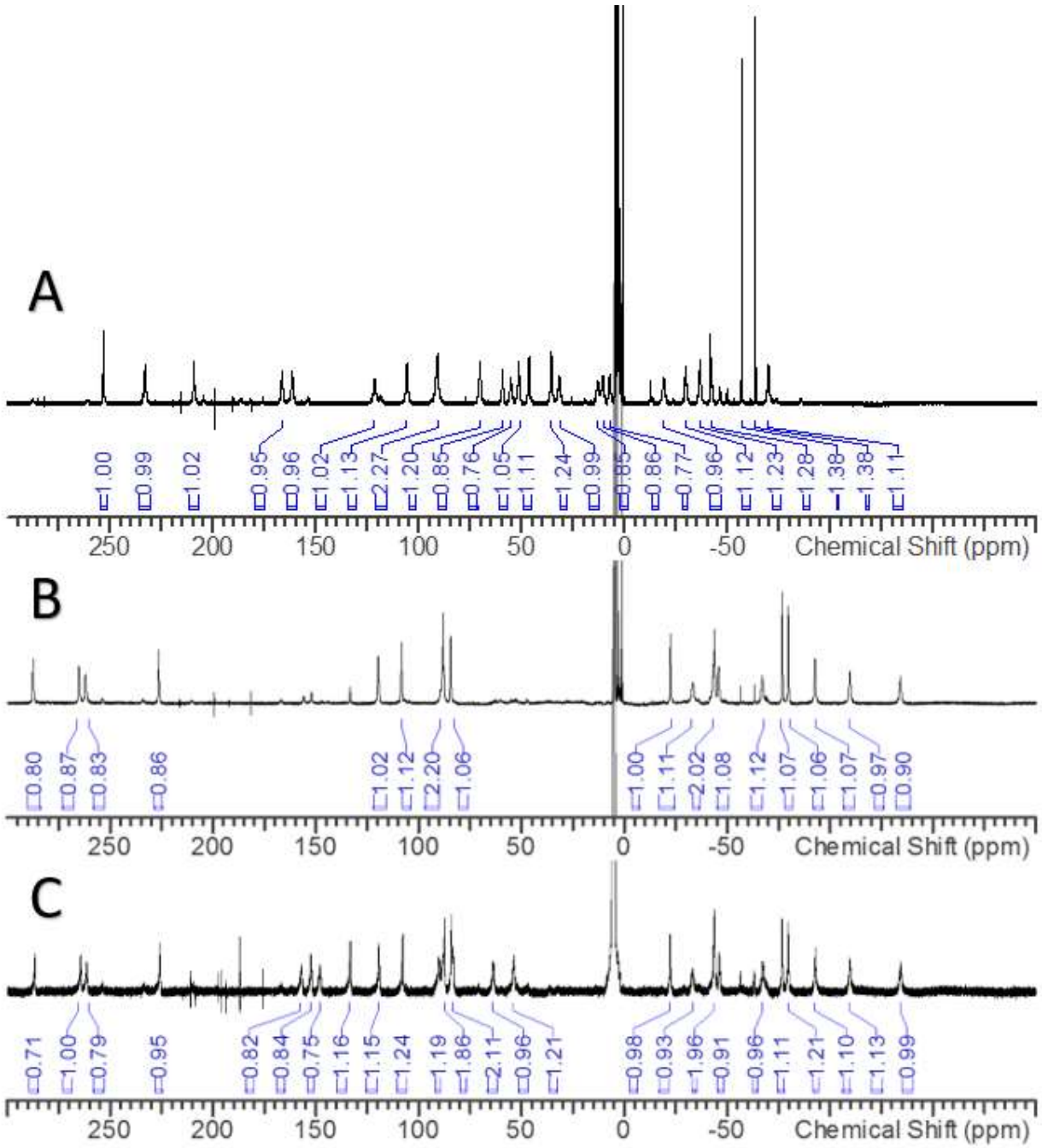

Figure S2: ^{1}H NMR spectra of a solutions of $[Co(CCRM)]^{2+}$ in D_2O; before heating (A), after heating (B), and a sample heated in H_2O to prevent deuterium exchange (C). A is associated with $[Co(1,4\text{-}CCRM)]^{2+}$, while B and C are associated with $[Co(1,8\text{-}CCRM)]^{2+}$.

Mass Spectrometry

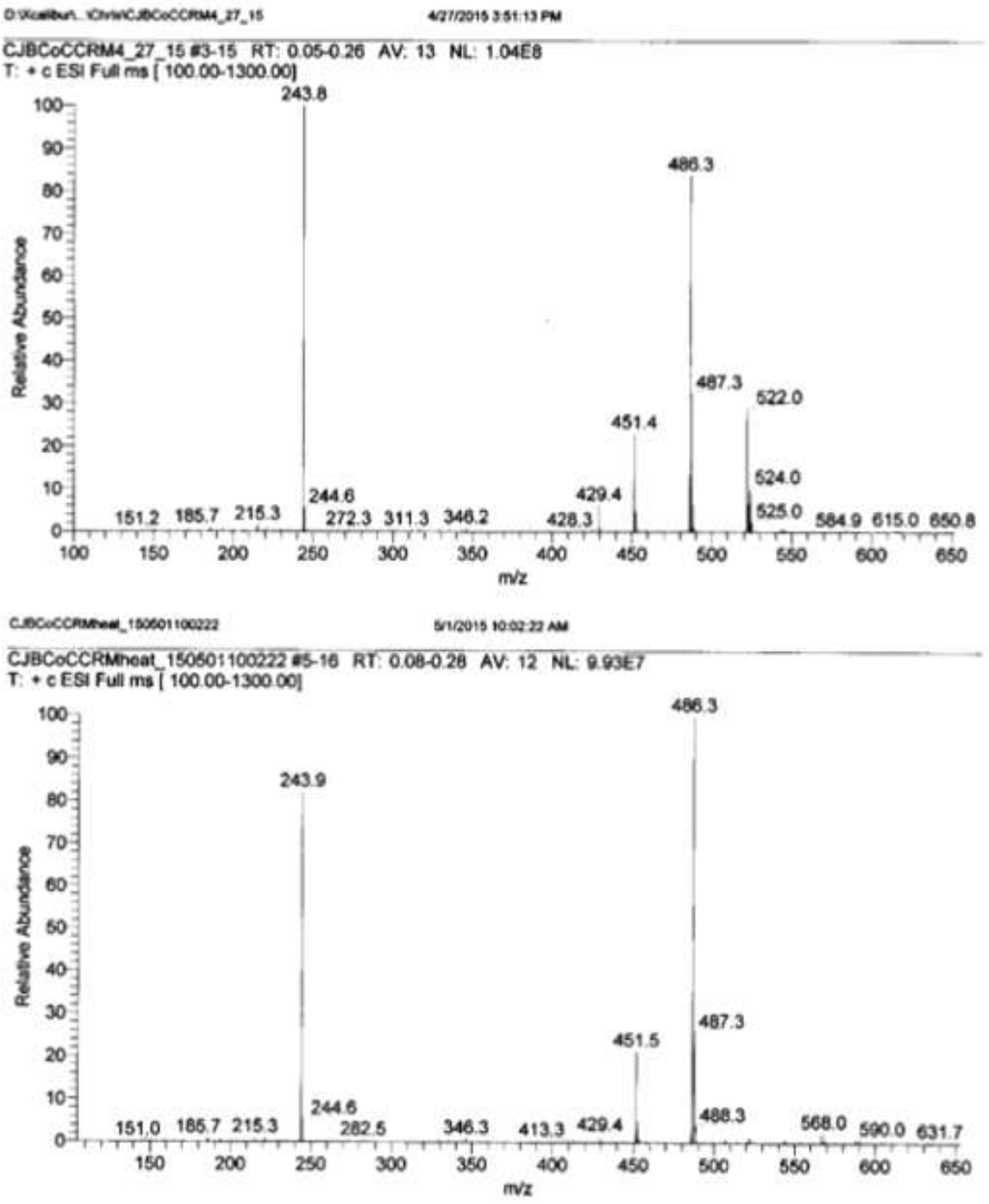

Figure S3: Mass spectra of $[Co(CCRM)]Cl_2$ top is before heating (I-1), and the bottom is after heating (I-2). Peaks of 243.8 and 486.3 m/z appear and 243.9 and 486.3 appeared for I-1 and I-2 respectively, corresponding to the $[Co(CCRM)]^{2+}$ and $[Co(CCRM\text{-}H+)]^{+}$ ions respectively. Minor peaks at 522 and 451 are $[Co(CCRM+Cl^{-})]^{+}$ and $[Na(CCRM)]^{+}$ respectively.

Table S2: Solution studies on $[Co(1,4\text{-CCRM})]^{2+}$ and $[Co(1,8\text{-CCRM})]^{2+}$ determining magnetic moment(μ_{eff}) (a), complex dissociation in acidic solution (b), complex dissociation in the presence of 25 mM HCO_3^{2-}, 0.4mM HPO_4^{3-} (c), dissociation in the presence of 20 mM (1 eq) of $ZnCl_2$(d), dissociation in the presence of Cu(II) (100 uM Co(II) complex), pH 6, 20 mM MES buffer(e). Values for a,b,c for $[Co(1,4\text{-CCRM})]^{2+}$ from literature.[1] The dissociation given for $[Co(1,8\text{-CCRM})]^{2+}$ is attributed to $[Co(1,4\text{-CCRM})]^{2+}$ impurity (15 ± 3%) resulting from incomplete isomerization**.**

Isomer	Magnetic moment (μ_{eff})	Acid dissociation (%)	Anion dissociation (%)	Dissociation with Zn(II)
$[Co(1,4\text{-CCRM})]^{2+}$	4.6	95	5	-
$[Co(1,8\text{-CCRM})]^{2+}$	4.7	10 ± 1*	2 ± 1*	9 ± 3*

*sample contained (15 ± 3%) of the $[Co(1,4\text{-CCRM})]^{2+}$ isomer

Acid dissociation

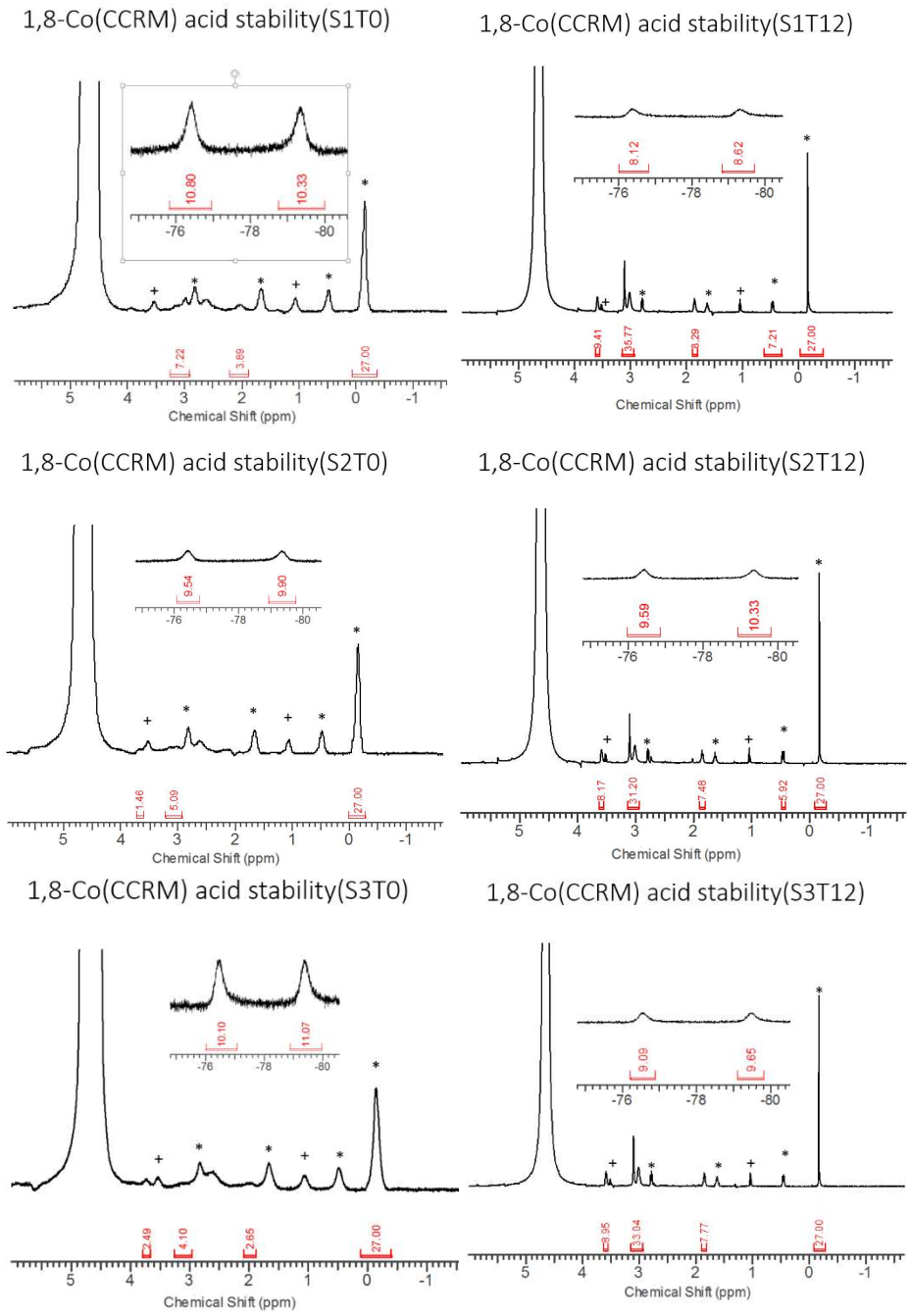

Figure S4: The dissociation of 20 mM of 1,8-CoCCRM in pD 3.5-4 solution was monitored before and after twelve hours in incubation at 37 ^{o}C by NMR using 3 mM Sodium 3-(trimethylsilyl)-1-propanesulfonate as an internal standard. Peaks appearing in the diamagnetic region during that time correspond to free CCRM ligand and the concentration was determined to calculate % dissociation. (Peaks labeled * correspond with 3-(trimethylsilyl)-1-propanesulfonate and peaks labeled + correspond to an ethanol impurity).

Anion (CO_3^{2-}, PO_4^{3-}) dissociation

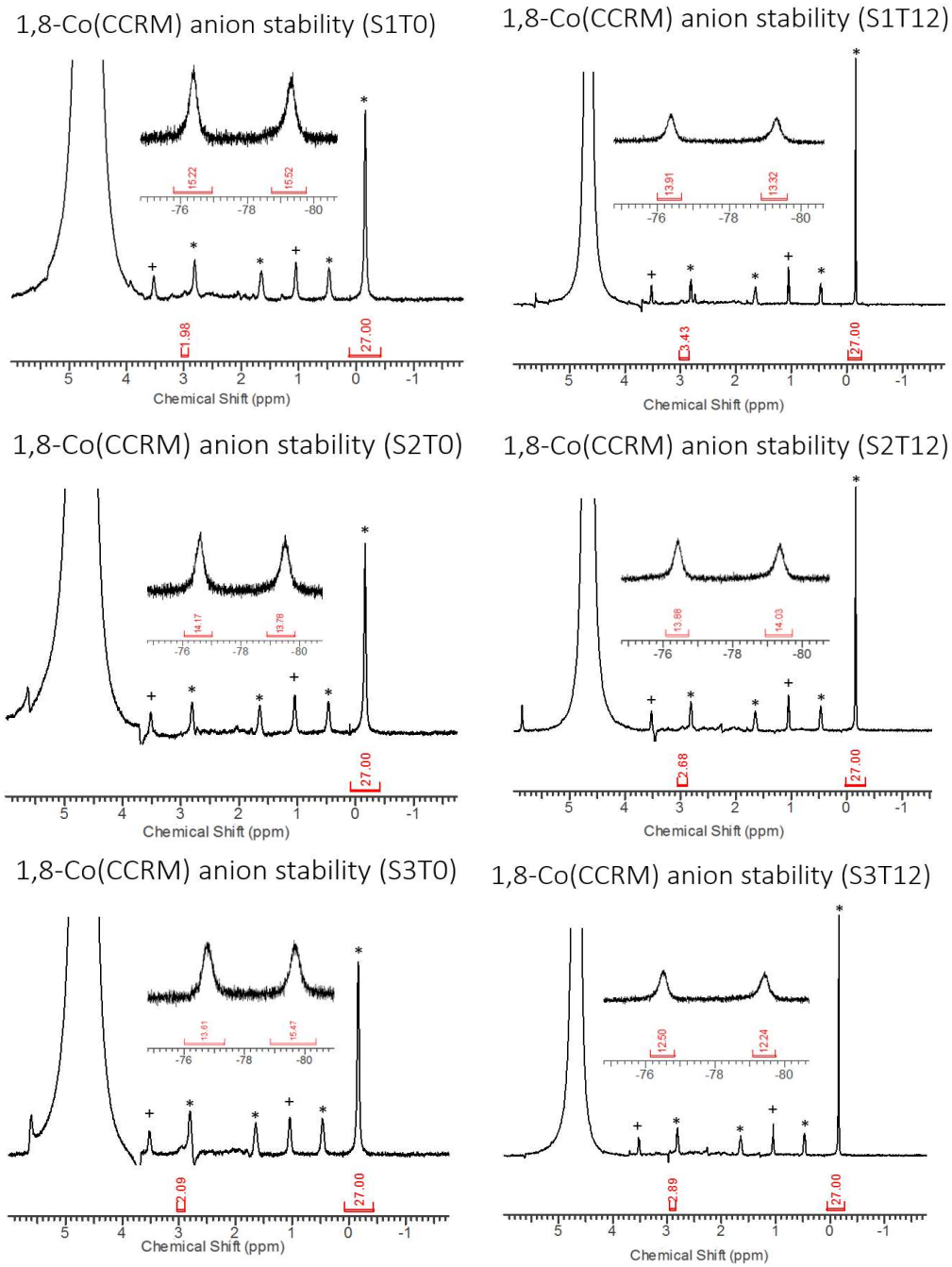

Figure S5: The dissociation of 20 mM of 1,8-Co(CCRM) in 25 mM bicarbonate, 0.4 mM hydrogen phosphate, pD 7.5 solution was monitored before and after twelve hours in incubation at 37 ^{o}C by NMR using 3 mM Sodium 3-(trimethylsilyl)-1-propanesulfonate as an internal standard. Peaks appearing in the diamagnetic region during that time correspond with free CCRM ligand and the concentration was determined to calculate % dissociation. (peaks labeled * correspond with 3-(trimethylsilyl)-1-propanesulfonate and peaks labeled + correspond to ethanol impurity).

Zn^{2+} Displacement Assay

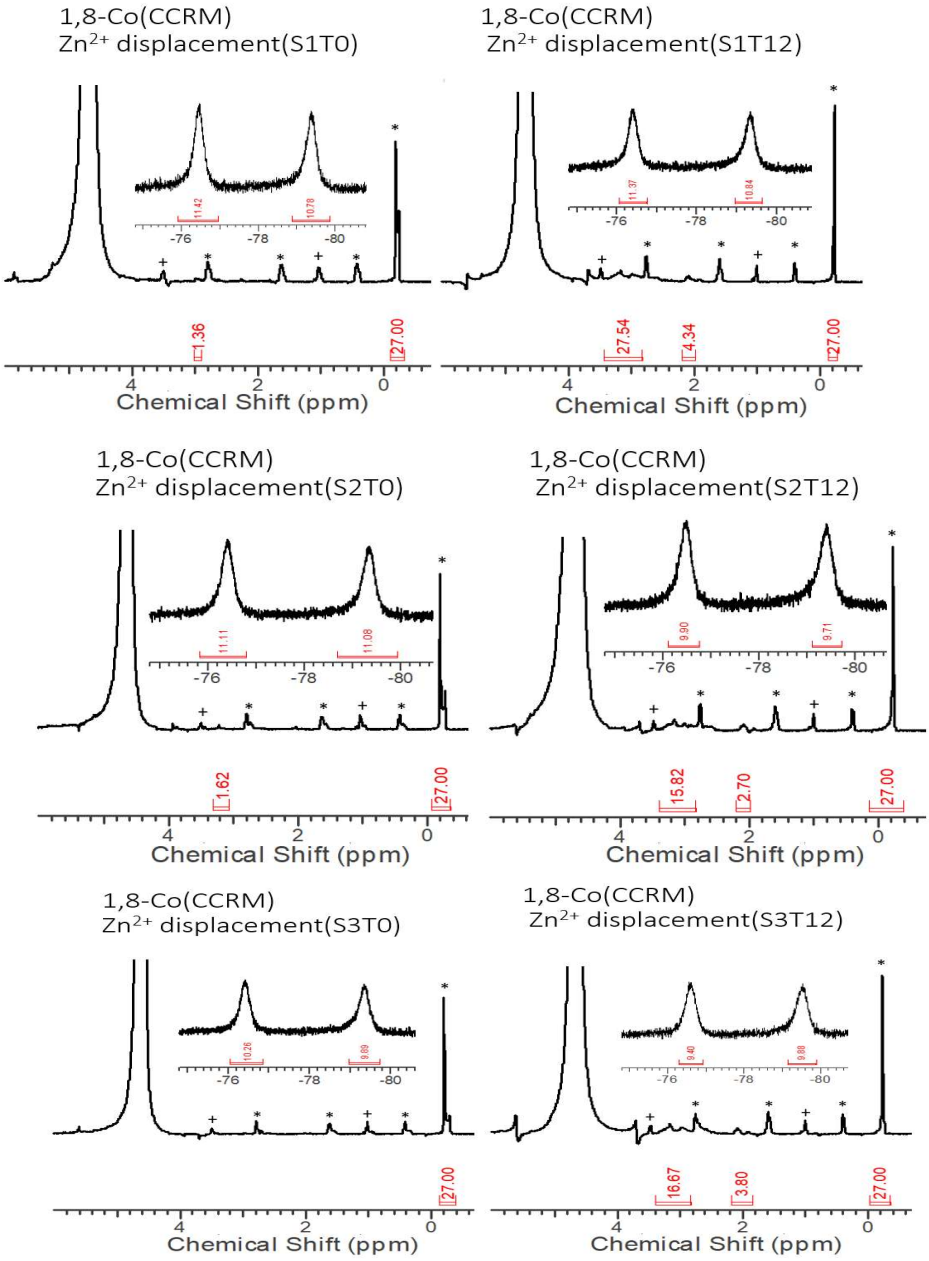

Figure S6: The dissociation of 20mM of 1,8-CoCCRM when an equivalent of $ZnCl_2$ was added and the solution was monitored before and after twelve hours in incubation at 37°C by NMR using 3mM Sodium 3-(trimethylsilyl)-1-propanesulfonate as an internal standard. Peaks appearing in the diamagnetic region during that time correspond with free CCRM ligand and the concentration was determined to calculate % dissociation. Peaks labeled * correspond with 3-(trimethylsilyl)-1-propanesulfonate and peaks labeled + correspond to small ethanol impurity.

Cu^{2+} displacement Assay

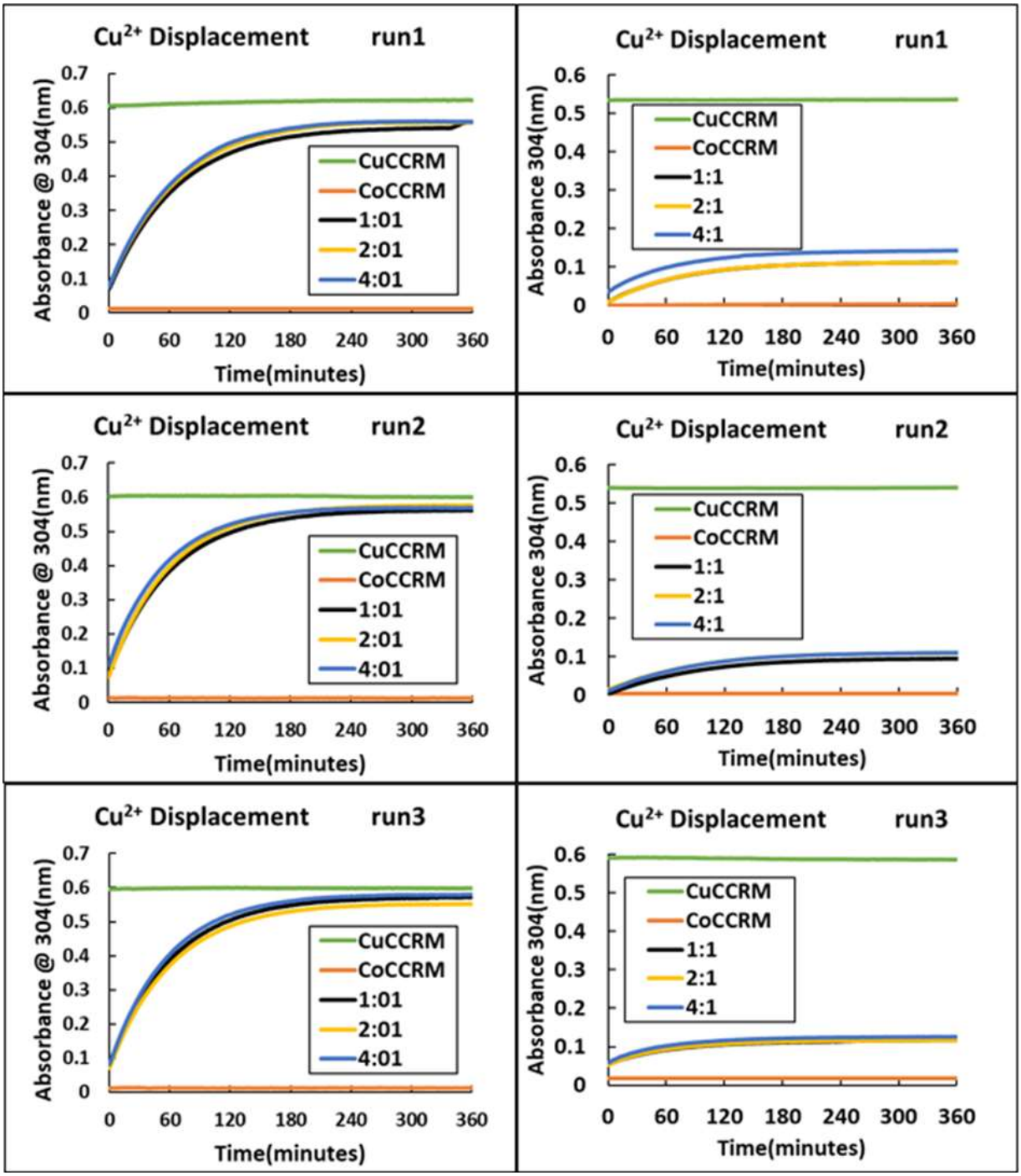

Figure S7: For dissociation resulting from Cu^{2+} transmetalation, solutions of 100 µM $[Co(CCRM)]^{2+}$ complex and 20 mM pH 6 MES buffer, had 1,2, or 4 equivalents of $Cu(NO_3)_2$ (aq) added, and the formation of $[Cu(CCRM)]^{2+}$ was observed overtime at one minute intervals by UV-vis at 304 nm. Percent dissociation was calculated using the following: absorbance of $[Co(CCRM)]^{2+}$ and $Cu(NO_3)_2$ solution/absorbance $[Cu(CCRM)]^{2+}$ after 6 hours, multiplied by 100%. For the Co(1,8-CCRM) isomer shown in right column, the Cu(II) displacement observed is attributed to a 15% impurity of $[Co(1,4\text{-}CCRM)]^{2+}$ as shown in left column.

Table S3: Transmetallation of Co(II) complex in the presence of $Cu(NO_3)_2$. For dissociation resulting from Cu^{2+} transmetalation, solutions of 100 µM Co(II) complex 20 mM pH 6 MES buffer, had 1,2, or 4 equivalents of $Cu(NO_3)_2$ (aq) added, and the formation of $[Cu(CCRM)]^{2+}$ was observed over time at one minute intervals by UV-vis at 304 nm at 25 °C. Percent dissociation was calculated using the following: 304 nm absorbance of $[Co(CCRM)]^{2+}$ and $Cu(NO_3)_2$ solution/absorbance $[Cu(CCRM)]^{2+}$ after 6 hours, multiplied by 100%. The trans-metallation reaction in the $[Co(1,8\text{-}CCRM)]^{2+}$ sample was attributed mostly to the presence of $[Co(1,4\text{-}CCRM)]^{2+}$ as an 15% ± 3% impurity.

Isomer	1:1 ratio $Cu(NO_3)_2$ to Complex	error	2:1 ratio $Cu(NO_3)_2$ to Complex	error	4:1 ratio $Cu(NO_3)_2$ to Complex	error
[Co(1,4-CCRM)]	93.0%	2.6%	92.5%	2.7%	93.8%	2.9%
[Co(1,8-CCRM)]*	19.5%*	1.5%	20.5%*	0.4%	22.9%*	2.7%

*sample contained 15% ± 3% $[Co(1,4\text{-}CCRM)]^{2+}$ isomer.

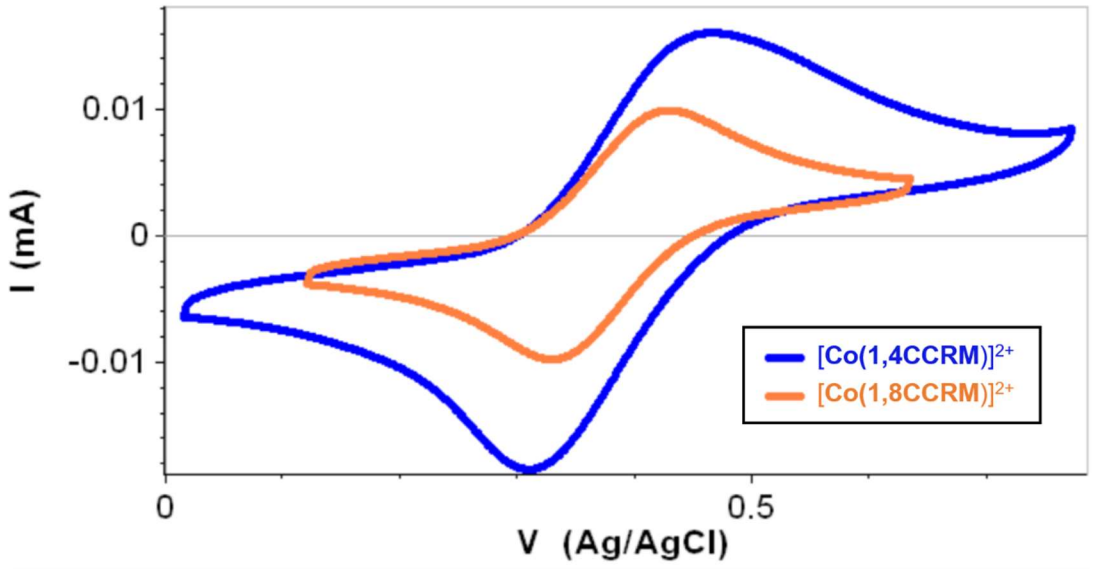

Figure S8. Overlaid cyclic voltammograms of $[Co(1,4\text{-}CCRM)]^{2+}$ and $[Co(1,8\text{-}CCRM)]^{2+}$, with milimolar complex, aqueous solution, 20 mM HEPES, 100 mM KCl at pH 7.0, 200 mV/s scan rate. Potentials measured vs. Ag/AgCl electrode with glassy carbon and platinum wire as working and counter electrodes respectively. $E_{1/2}$= of 389 mV and 380 mV vs. Ag/AgCl and 551 mV and 542 mV vs. SHE respectively.

Electronic spectroscopy

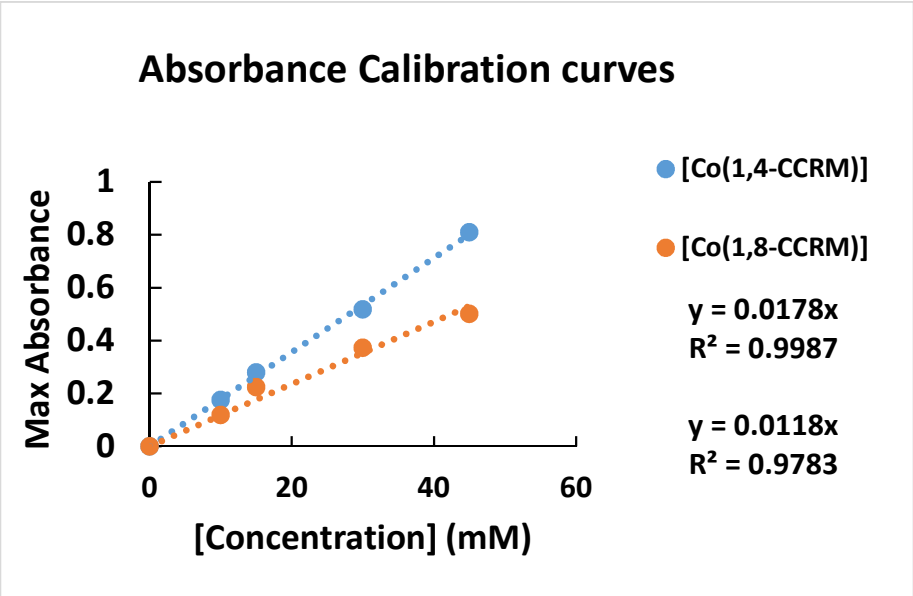

Figure S9: Absorbance and as a function of concentration of complex with $[Co(1,4\text{-}CCRM)]^{2+}$ at 493 nm (blue), and $[Co(1,8\text{-}CCRM)]^{2+}$ at 487nm (orange), 10 to 50 mM samples in water. Slopes indicate molar absorptivity of 17.8 and 11.8 L mol^{-1} cm^{-1} respectively.

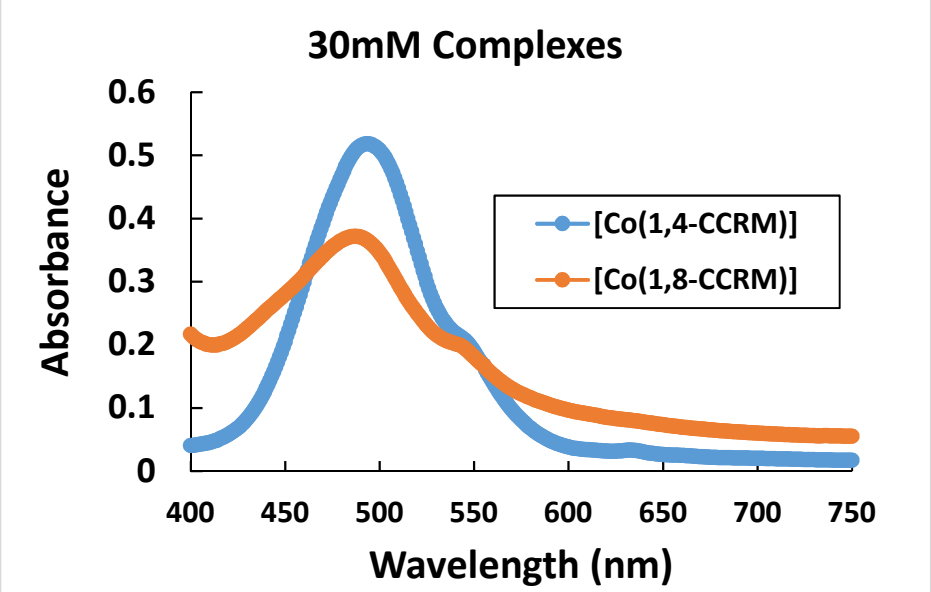

Figure S10: UV-vis spectra of isomers $[Co(1,4\text{-}CCRM)]^{2+}$ (blue) and $[Co(1,8\text{-}CCRM)]^{2+}$ orange from 400 to 750 nm, 30 mM samples in water.

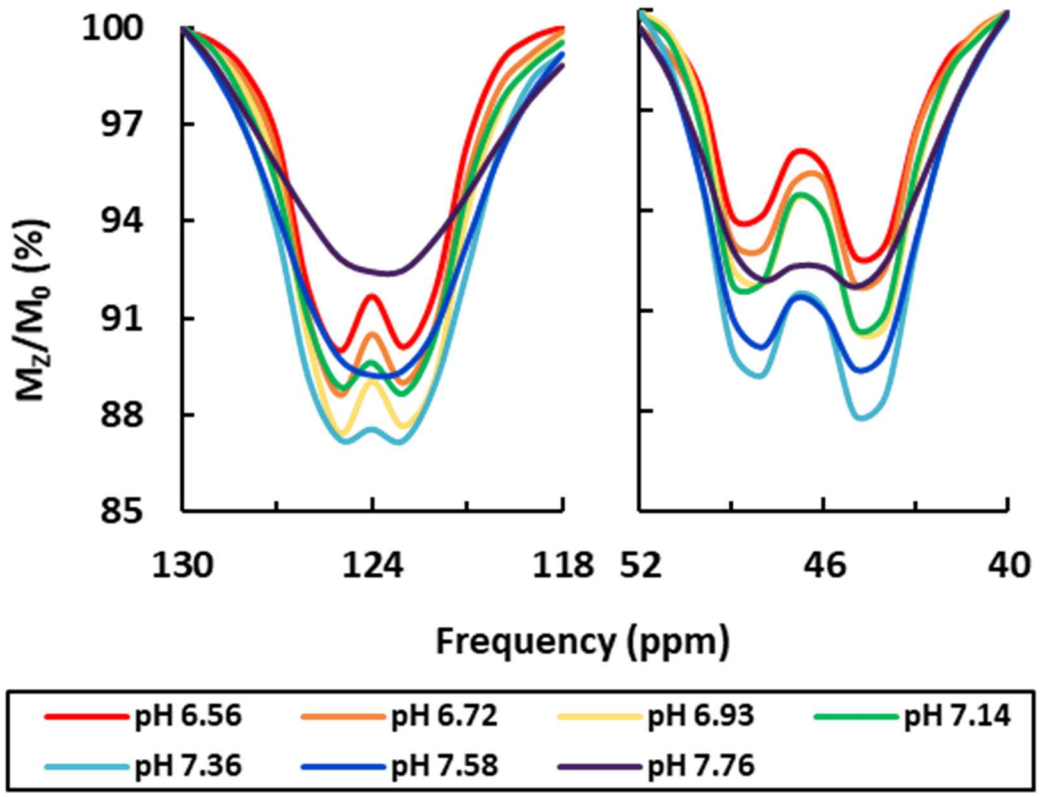

Figure S11: Z-spectra taken at 37 °C of $[Co(1,8\text{-CCRM})]^{2+}$, B_1 = 12.7 µT at 11.7 T. The sample contained 10 mM complex, 20 mM pH 7.40 HEPES buffer, and 100 mM NaCl. The pH values varied between 6.6 and 7.8.

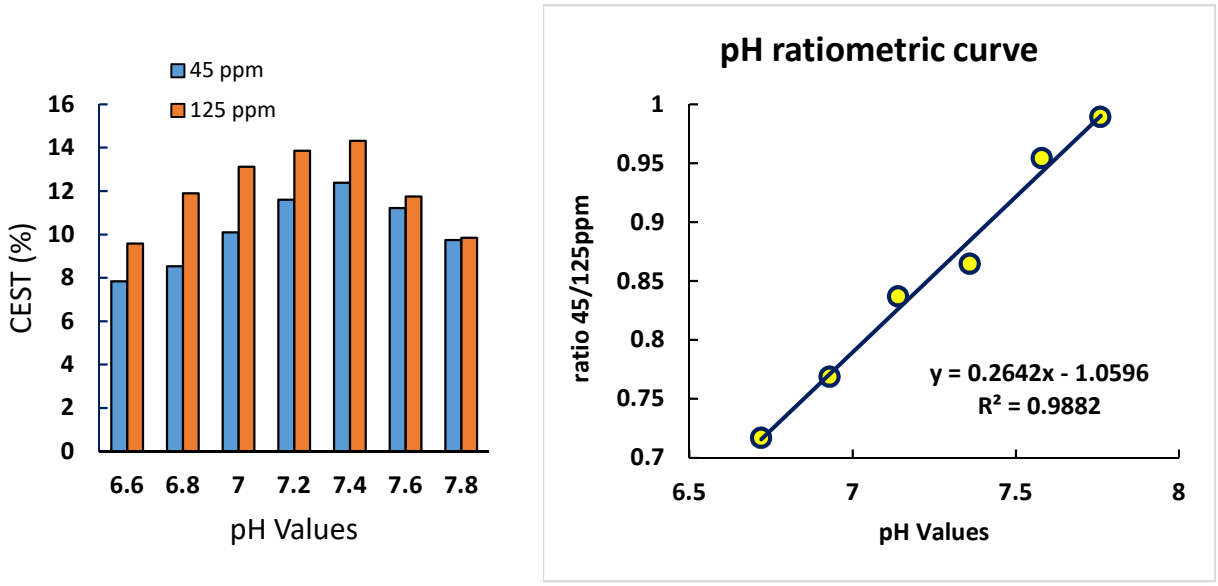

Figure S12: The saturation transfer (ST= (1-M_Z/M_0) x100) is plotted as a function of pH (bottom left), and the ratio of the CEST peaks (45 ppm/125 ppm) at a given pH value is plotted at bottom right. B_1 = 12.7 µT at 11.7 T. The sample contained 10 mM complex, 20 mM pH 7.40 HEPES buffer, and 100 mM NaCl.

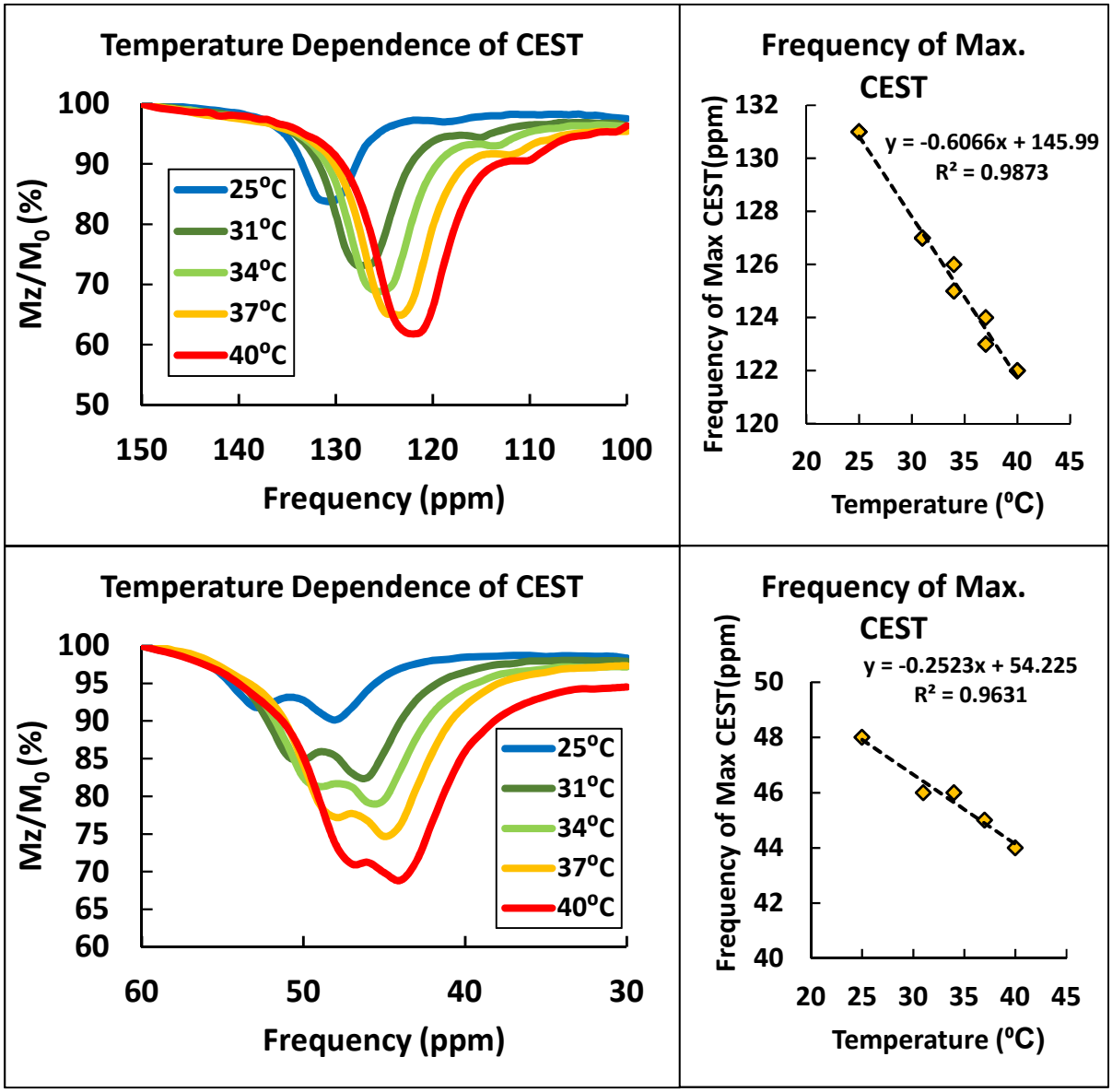

Figure S13: Z-spectra (left) of $[Co(1,8\text{-CCRM})]^{2+}$ at pH 7.2, 10 mM complex, 20 mM pH 7.2 HEPES buffer, 100 mM NaCl, varying temperatures between 25 and 40 °C, 29 µT. Corresponding C_T plots on the right, monitoring the change in the frequency of the CEST peak as a function temperature.

Table S4: Exchange rate constants (k_{ex} s^{-1}) for $[Co(1,8\text{-CCRM})]^{2+}$ at 125 and 45 ppm calculated with HW-Quesp method. Solutions contained 10 mM complex, 20 mM HEPES buffer, and 100 mM NaCl, and at pH values between 6.6 and 7.8, with power varied from 4.0-12.7μT.

pH	k_{ex} 45ppm	Stand dev	pH	k_{ex} 125ppm	Stand dev
6.6	270	30	6.6	380	20
6.8	320	40	6.8	440	10
7.0	380	30	7.0	530	10
7.2	490	30	7.2	660	10
7.4	600	50	7.4	900	160
7.6	890	80	7.6	1100	100
7.8	1100		7.8	1600	

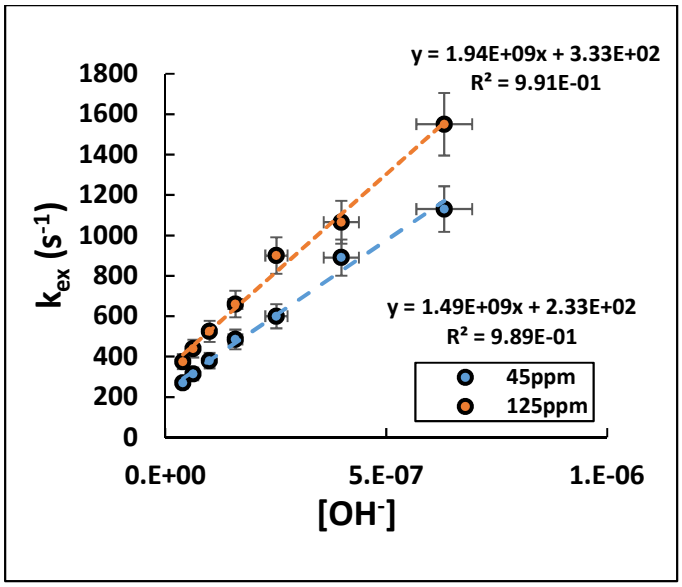

Figure S8: A plot of exchange rate constants (k_{ex}) obtained from the HW-Quesp method vs. $[OH]^-$ for Co(1,8-CCRM) CEST peaks at 125 and 45 ppm.

MRI Phantoms

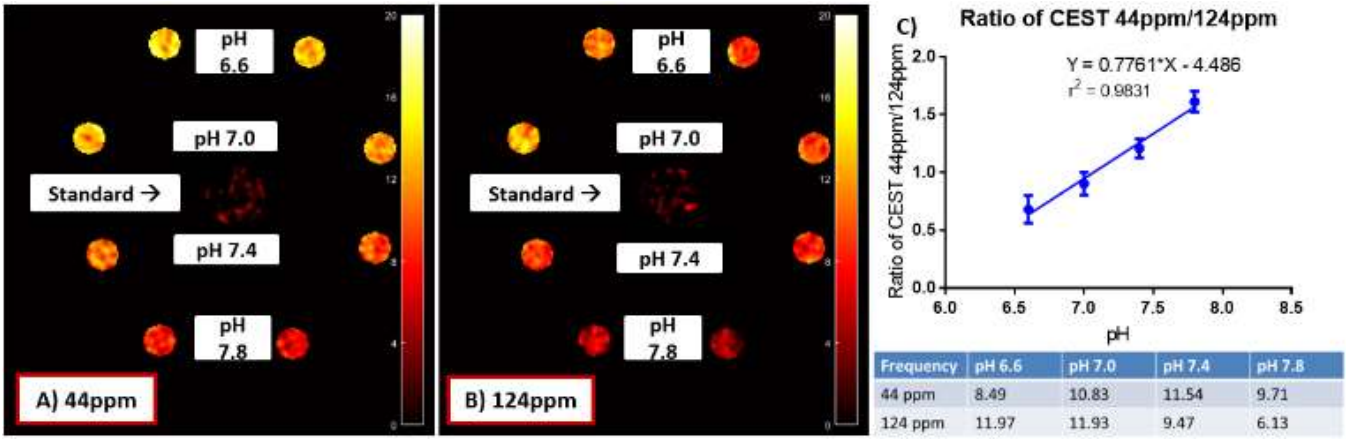

Figure S9: MRI phantom images of solutions containing 10 mM $[Co(1,8\text{-CCRM})]^{2+}$, 20 mM buffer, and 100 mM NaCl, with pH values of 6.6(MES buffer), 7,7.4, and 7.8 (HEPES buffer), with presaturation pulse applied at 44 ppm (A) and 124 ppm (B) away from bulk water at 12 µT. Note that there are two samples for each pH value, and a buffer standard in the center of each image. The percent CEST was calculated and used to produce a ratiometric plot (C).

Chicken tissue homogenate study.

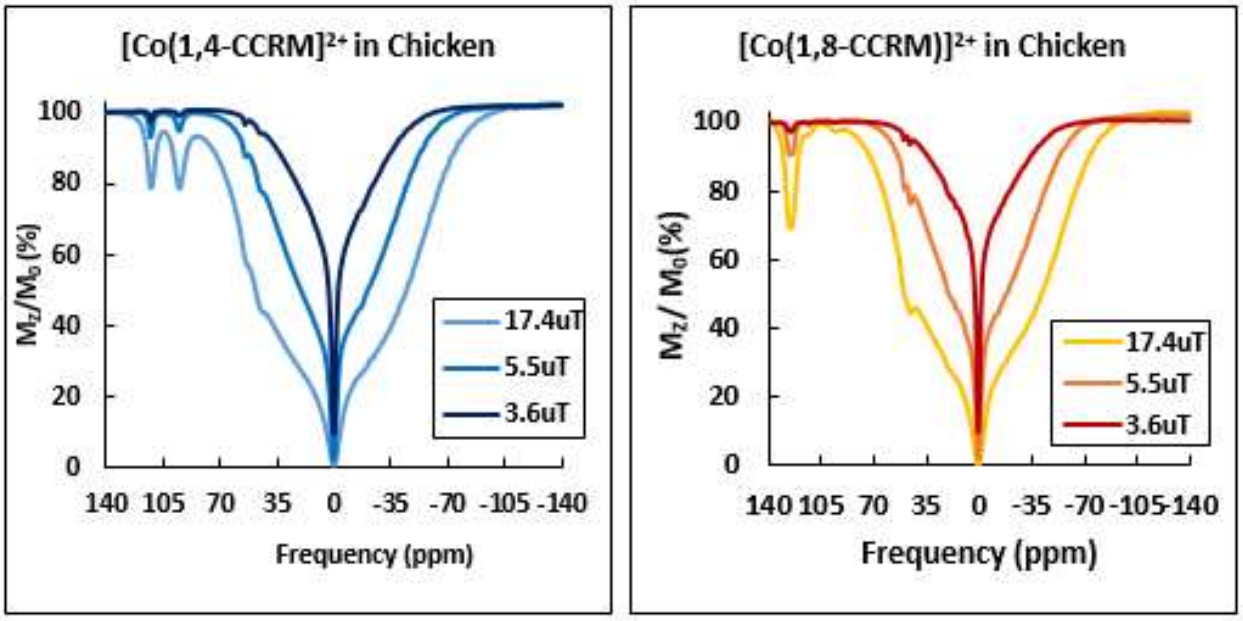

Figure S16: Z-spectra and CEST peaks of chicken samples soaked with $[Co(1,4\text{-}CCRM)]^{2+}$ (left) and $[Co(1,8\text{-}CCRM)]^{2+}$ (right), acquired at 3.6, 5.5, and 17.4 µT at 500 MHz for comparison. The pH of the samples were measured to be 7.2 and 6.9 respectively.

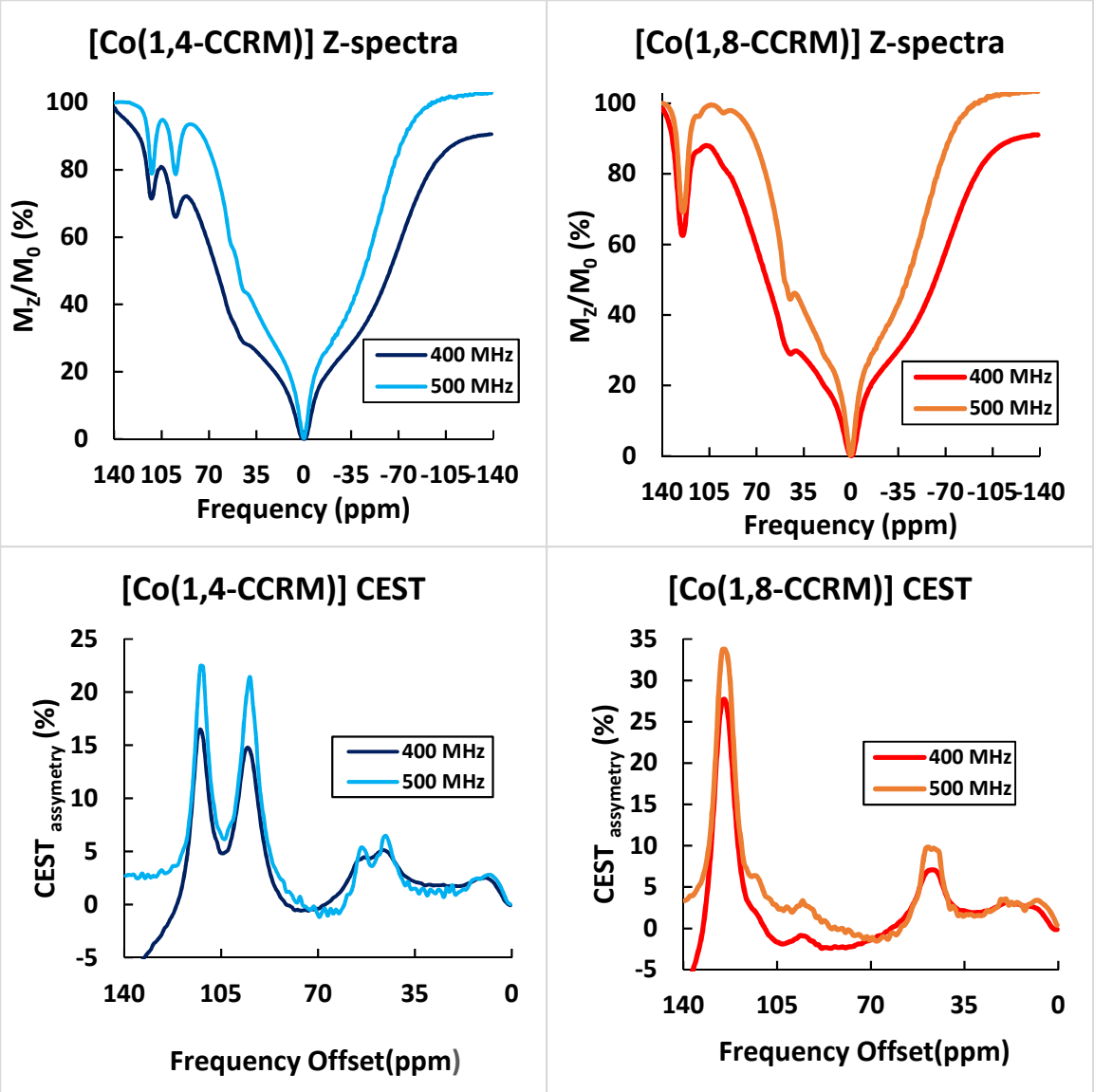

Figure S10. Z-spectra and CEST peaks of chicken samples soaked with $[Co(1,4\text{-CCRM})]^{2+}$ (left) and $[Co(1,8\text{-CCRM})]^{2+}$ (right), 55 mM solutions, acquired at on 400 and 500 MHz NMR spectrometers for comparison. B_1=17.4 µT. The pH of the samples were measured to be 7.2 and 6.9 respectively.

Tissue Studies; Omega Plots and Exchange Rates

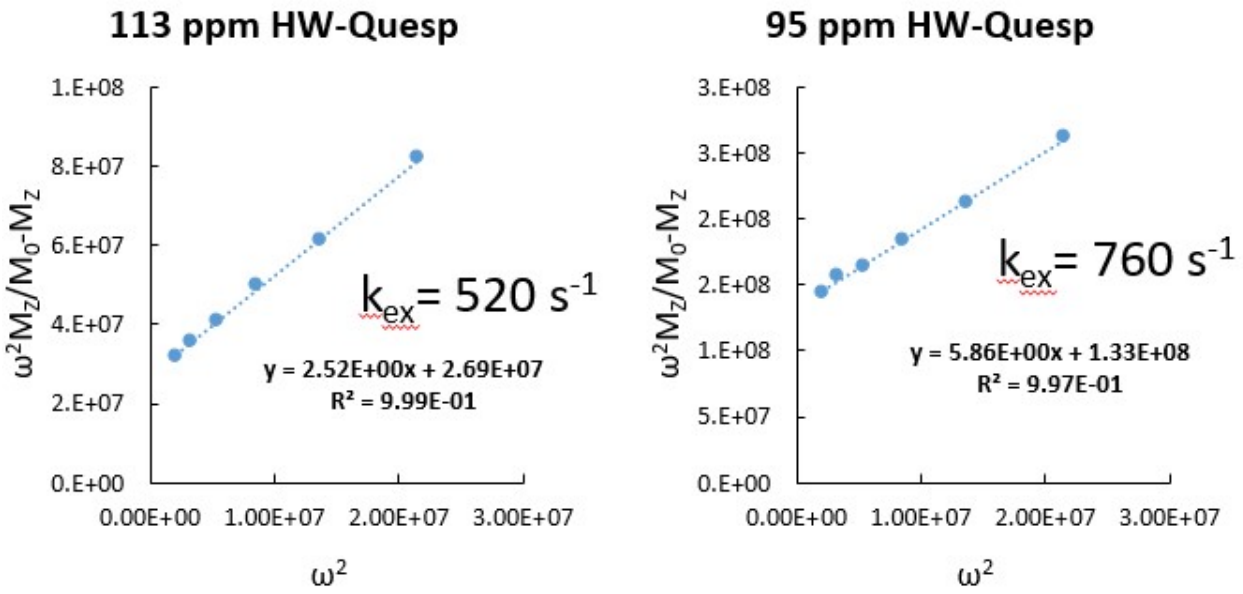

Figure S11: The HW-Quesp at 113 and 95 ppm of (M_Z/(M_0 - M_Z) vs. (1/ω^2) of $[Co(1,4\text{-CCRM})]^{2+}$ soaked chicken sample at pH 7.39. Radiofrequency pulse applied for 2 seconds while varying B_1 between 3.9-12.4 µT. M_Z is at the frequency of interest, and M_0 was applied at (M_Z+16ppm). Exchange rate constants of 520 s^{-1} and 760 s^{-1} respectively were calculated.

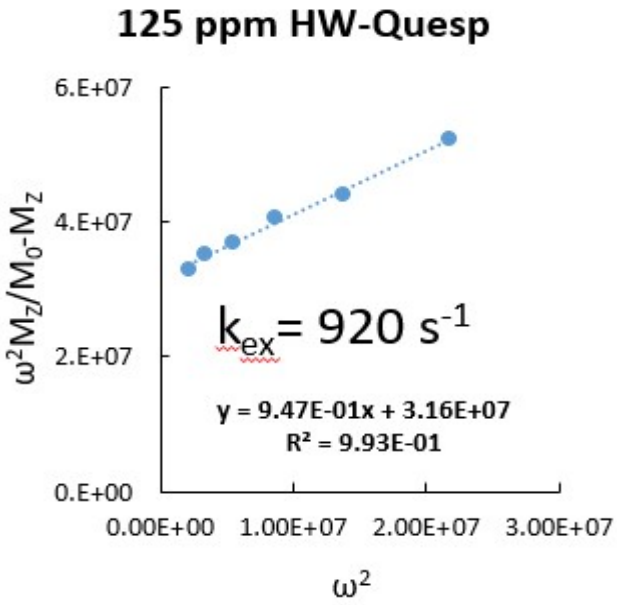

Figure S19: The HW Quesp at 125 ppm of (M_Z/(M_0 - M_Z) vs. (1/ω^2) of $[Co(1,8\text{-CCRM})]^{2+}$ soaked chicken sample at pH 7.40. Radiofrequency pulse applied for 2 seconds while varying B_1 between 3.9-12.4 µT. M_Z is at the frequency of interest, and M_0 was applied at (M_Z+16ppm). Exchange rate constants of 860 s^{-1} respectively were calculated.

pH studies in chicken homogenate and exchange rate constants.

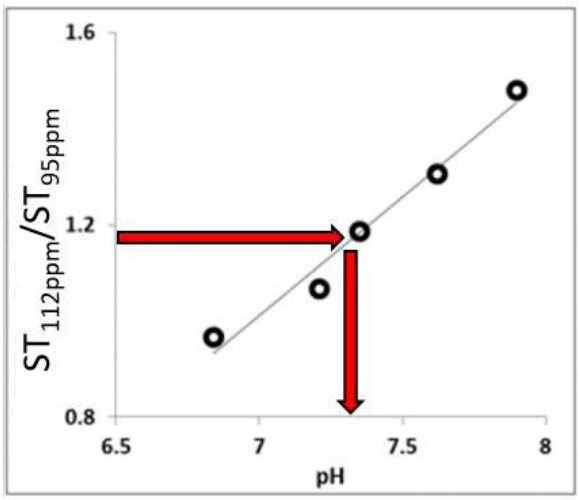

	k_{ex} (s^{-1})		
	pH 7.0	pH 7.4	pH 8.0
112 ppm	300 ± 40	510 ± 20	1550 ± 10
95 ppm	540 ± 10	910 ± 20	2100 ± 250
54 ppm	380 ± 20	440 ± 20	920 ± 40
45ppm	480 ± 10	780 ± 40	1760 ± 40

Figure S20: Ratiometric plot and exchange rate constant values of $[Co(1,4\text{-}CCRM)]^{2+}$ from literature[1], used to analyze the ability of the complex to report pH in the presence of chicken. For the sample of [Co(1,4-CCRM)], in chicken breast, featured in Figure 4, the measured pH value was 7.39. The ratio of ST_{112}/ST_{95}= 1.18, close to the value of 1.2 depicted in the graph (left). The k_{ex} at 112-113ppm= 520 s^{-1} (determined from HW-quesp in Figure S17), matches pH 7.4 value within error from literature (right). The k_{ex} at 95ppm =760 s^{-1}, (determined from HW-quesp), value in-between expected values pH 7.0 and pH 7.4 from literature (right).[1]

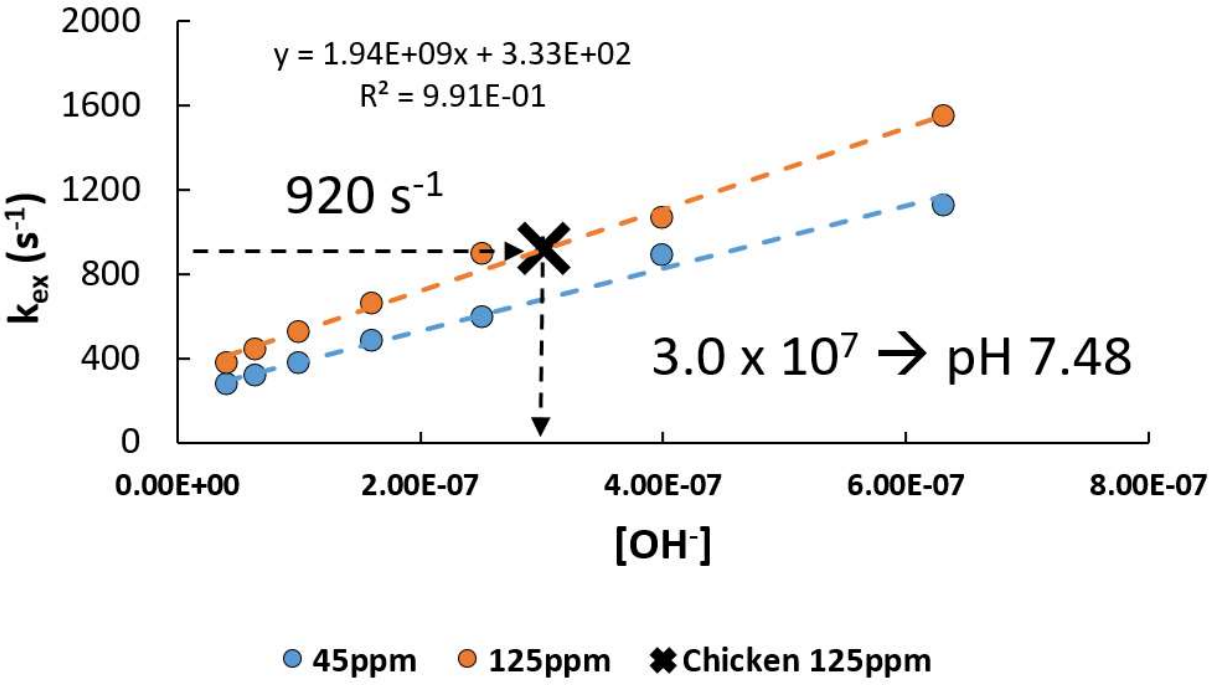

Figure S12: A plot of exchange rate constants (k_{ex}) obtained from the HW-Quesp method vs. $[OH]^-$ for Co(1,8-CCRM) CEST peaks at 125 and 45 ppm, adapted from Figure S13. The value of k_{ex}= 920 s^{-1} obtained for HW-Quesp (Figure S18). This value corresponds to 900s^{-1} at pH 7.4 values on table S4, and corresponds with a pH value of 7.48 if using the fitted equation shown above. For [Co(1,8-CCRM)], in chicken breast, the measured pH value was 7.40.

The ST Ratio 45ppm/125ppm = 0.379, fitting to a pH of 5.5 according the ratiometric parameters from figure S12. Interference from the MT effect obscured signal at 45 ppm, resulting in the inaccurate ratiometric determined pH of 5.5.

Appendix

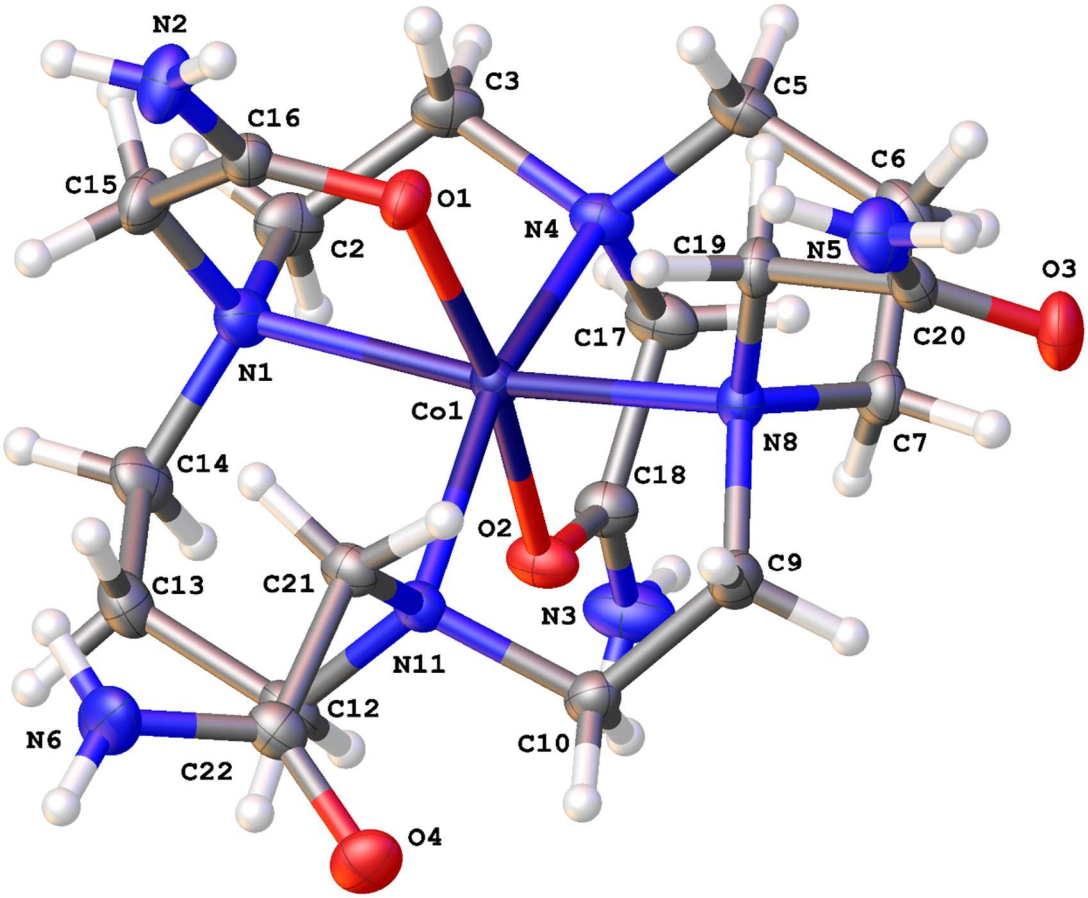

Figure A 1: A crystal structure of the complex cation of $[Co(1,4\text{-}CCRM)](ClO_4)_2 \cdot H_2O$.

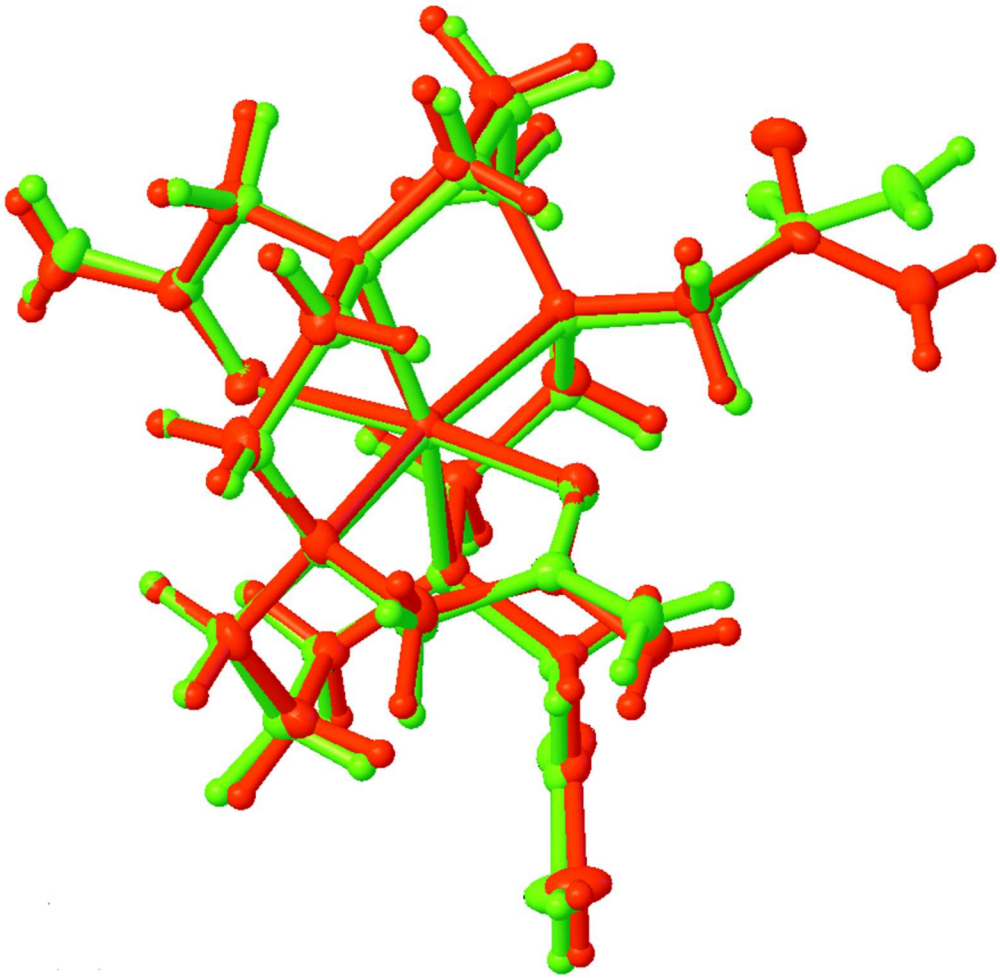

Figure A 2 : Overlapping structures of the cations of $[Co(1,4\text{-}CCRM)]^{2+}$ from complexes with different counterions.

References:

1. Dorazio, S. J.; Olatunde, A. O.; Spernyak, J. A.; Morrow, J. R., CoCEST: cobalt(II) amide-appended paraCEST MRI contrast agents. *Chem Commun* **2013,** *49* (85), 10025-10027.
2. Dixon, W. T.; Ren, J.; Lubag, A. J. M.; Ratnakar, J.; Vinogradov, E.; Hancu, I.; Lenkinski, R. E.; Sherry, A. D., A concentration-independent method to measure exchange rates in PARACEST agents. *Magnet Reson Med* **2010,** *63* (3), 625-32.
3. Randtke, E. A.; Chen, L. Q.; Corrales, L. R.; Pagel, M. D., The Hanes-Woolf linear QUESP method improves the measurements of fast chemical exchange rates with CEST MRI. *Magnet Reson Med* **2014,** *71* (4), 1603-12.
4. Piguet, C., Paramagnetic susceptibility by NMR: The ''solvent correction'' removed for large paramagnetic molecules. *J Chem Educ* **1997,** *74* (7), 815-816.
5. Evans, D. F., The Determination of the Paramagnetic Susceptibility of Substances in Solution by Nuclear Magnetic Resonance. *J Chem Soc* **1959,** (Jun), 2003-2005.
6. Sheldrick, G. M., Crystal structure refinement with SHELXL. *Acta Crystallographica Section C-Structural Chemistry* **2015,** *71*, 3-8.
7. Sheldrick, G. M., SHELXT - Integrated space-group and crystal-structure determination. *Acta Crystallogr A* **2015,** *71*, 3-8.
8. Krause, L.; Herbst-Irmer, R.; Sheldrick, G. M.; Stalke, D., Comparison of silver and molybdenum microfocus X-ray sources for single-crystal structure determination. *J Appl Crystallogr* **2015,** *48*, 3-10.
9. Dolomanov, O. V.; Bourhis, L. J.; Gildea, R. J.; Howard, J. A. K.; Puschmann, H., OLEX2: a complete structure solution, refinement and analysis program. *J Appl Crystallogr* **2009,** *42*, 339-341.